9

The Seismology of the Planet Mongo: The 2015 Ionospheric Seismology Review

Giovanni Occhipinti

ABSTRACT

The catastrophic seismic events of the last decades push forward the necessity to explore new techniques for source estimation, oceanic tsunami tracking, as well as tsunami warning systems. Early observations of the Rayleigh wave signature in the ionosphere by Doppler sounder were able to measure lithospheric properties, sounding the atmosphere at 200 km of altitude. After the Sumatra event (26 December 2004), the successful tsunami detection by altimeters validates the possibility of tsunami detection by ionospheric sounding. Today, the catastrophic tsunamigenic earthquake in Tohoku (11 March 2011) strongly affirms the potential of ionospheric sounding to visualize the vertical displacement of the ground and ocean: the Japanese GPS network, GEONET, imaged the source extent 8 min after the rupture; it also visualizes the radiation pattern and Rayleigh waves over the entire Japan, including the oceanic region overlooking the rupture; in the far field, the airglow camera located in Hawaii showed the internal gravity wave forced by the tsunami propagating in a zone of $180 \times 180\,km^2$ around the island. The ionospheric sounding potential of 2D visualization could extend the present vision of seismology. This work highlights the actual capability and the potential improvement suggested by ionospheric seismology.

9.1. ORIGINS

In early history, *Aristoteles* [524] described his pneumatic theory that the cause of earthquake is the *pneuma*, and indirectly the atmosphere: indeed, the wind, heated by the Sun, gets inside the Earth-cavities where it produces strong pressure variations resulting in the earthquake. The simplistic (and unrealistic) vision of *Aristoteles* [524] contains the visionary idea about the unicity of the Earth: solid Earth and the fluid parts of the planet, nominally the ocean and the atmosphere/ionosphere, continuously exchange energy. Today, the continuous excitation of normal modes, observed in the solid Earth by seismometers and usually called the "hum," is the clear proof of this hypothesis [*Nawa et al.*, 1998; *Suda et al.*, 1998; *Tanimoto et al.*, 1998; *Roult and Crawford*, 2000; *Kobayashi et al.*, 2001]. Several observational works show that the source of the hum is located mainly in the ocean [*Rhie and Romanowicz*, 2004; *Webb*, 2007] and partially in the atmosphere [*Nishida et al.*, 2000]. In particular, the atmospheric component of the hum seams to excite normal modes ${}_0S_{29}$ and ${}_0S_{37}$.

An additional proof of the coupling between the solid Earth and the atmosphere is the volcanic explosion of Mount Pinatubo in 1991. The atmospheric explosion was detected worldwide by the global network of seismometers in the form of a bichromatic signal with energy mainly located at 3.68 mHz and 4.40–4.65 mHz, corresponding to normal modes ${}_0S_{27-29}$ and ${}_0S_{34-37}$ [*Kanamori and Mori*, 1992; *Zurn and Widmer*, 1996; *Watada and Kanamori*, 2010].

In essence, the atmospheric energy excited by the volcanic explosion or by the atmospheric dynamics (hum-source) is transferred inside the solid Earth where it propagates at the surface as Rayleigh waves, detectable by seismometers.

Institut de Physique du Globe de Paris, Sorbonne Paris Cité, Universit Paris Diderot, France

Subduction Dynamics: From Mantle Flow to Mega Disasters, Geophysical Monograph 211, First Edition.
Edited by Gabriele Morra, David A. Yuen, Scott D. King, Sang Mook Lee, and Seth Stein.

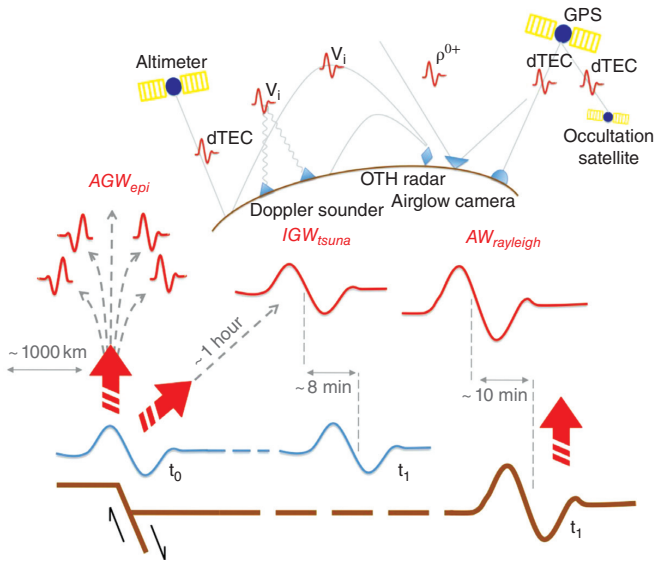

Figure 9.1 Schematic view of the coupling mechanism (bottom) and the ionospheric sounding techniques (top). Ground and oceanic displacement at the source produces AGW_{epi} that are observable in the ionosphere ~8 min after the rupture and observable until ~1000 km from the epicenter. The oceanic displacement initiates the tsunami that, during its propagation, creates IGW_{tsuna} that reach ionosphere in ~1* hr and keeps a delay of ~8* min compared to the tsunami at the sea surface. At teleseismic distance, the Rayleigh wave induces $AW_{Rayleigh}$ propagating vertically to the ionosphere in ~10 min. Times marked (*) are computed for a tsunami with a main period of 10 min, see *Occhipinti et al*. [2013] for different periods. Ionospheric sounding techniques (observable): Doppler sounder and OTH radar (vertical ion velocity); Altimeter and GPS (perturbation of the TEC), airglow (O^+ density perturbation).

Successive theoretical works [*Watada*, 1995; *Lognonné et al.*, 1998] strongly support this coupling observations and explain that the energy can be transferred in two ways: from the solid Earth to the atmosphere and *vice versa*. Normal modes computed for the Earth with ocean and atmosphere [*Lognonné et al.*, 1998] clearly show that Rayleigh waves produce acoustic waves in the atmosphere (see section 2); in the same way, tsunamis produce internal gravity waves in the overlying atmosphere (see section 4). Here we indicate the first with $AW_{Rayleigh}$ and the second IGW_{tsuna} (Figure 9.1).

The first observational evidence of the coupling between solid Earth and the fluid envelopes of the planet is an indirect consequence of the Cold War: the continuous monitoring to detect nuclear explosions via their signature in the atmosphere and in the solid Earth pushed scientists and engineers to compare atmospheric/ionospheric observations (barometers, Doppler sounders, and backscattered radars) with data from seismometers. This data matching from different instruments revealed that acoustic-gravity waves are generated not only after nuclear explosions but also after seismic events [*Row*, 1967]. As a consequence of the rich spectrum of energy characterizing the seismic rupture, the ground displacement at the epicenter (Figure 9.1) generates, simultaneously, acoustic and gravity waves in the atmosphere above the epicenter (AGW_{epi}).

After the Alaska earthquake in 1964 ($M\omega$ 9.2), the Berkeley barometer detected two unexpected signals: the first was correlated with the arrival time of Rayleigh wave ($AW_{Rayleigh}$), the second was essentially an acoustic-gravity wave propagation from the epicenter (AGW_{epi}) [*Bolt*, 1964]. The atmospheric waves propagate through the low neutral atmosphere [*Donn and Posmentier*, 1964] and up to the ionosphere where they are detected by ionospheric sounding [*Davies and Baker*, 1965; *Leonard and Barnes*, 1965; *Row*, 1966]. The 1964 Alaska earthquake opened the era of ionospheric seismology.

9.2. IONOSPHERIC SEISMOMETERS

Many observations followed the 1964 Alaska event and clearly showed that the signature of Rayleigh waves was detectable by ionospheric monitoring, mainly using Doppler sounders.

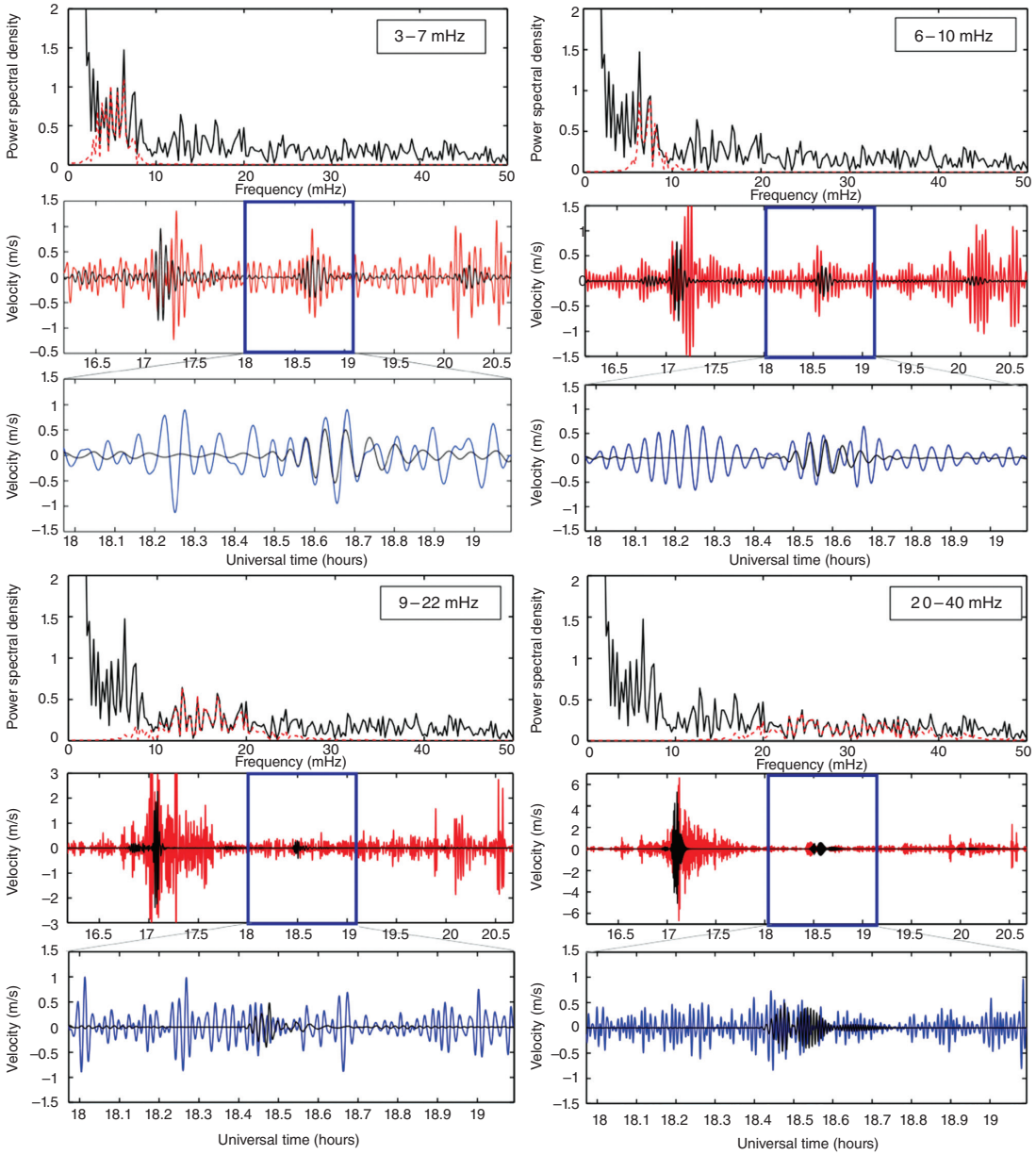

AQ3

Figure 9.2 Spectral analysis of the $AW_{Rayleigh}$ detected by Doppler sounder and OTH radar after the Sumatra event (28 April 2005, M_{ω} 8.1). In each triptych (three plots for each highlighted band-pass range): top, spectrum of the Doppler sounder raw-data (black) and band pass filtered data (red dotted) in the frequency range showed in the right corner. Middle, Doppler sounder filtered data (red) and modeling (black), showing clearly R1 and R2, and sometimes a clear signature of R3. Bottom, OTH radar filtered data (blue) and modeling (black) showing only R2 (the timescale corresponds to the blue square in the middle plot). The R1 $AW_{Rayleigh}$ in the Doppler sounder is still recognizable independent of the frequency range; the signature of R2 $AW_{Rayleigh}$ that after 10 mHz.

In essence, the vertical ground displacement at the epicenter or at teleseismic distance (induced by Rayleigh waves) generates, by dynamic coupling, an acoustic-gravity wave that propagates in the neutral atmosphere. During the wave upward propagation, the wave is strongly amplified by the coupled effect of the conservation of kinetic energy $E_k = \frac{1}{2}\rho v^2$ and the exponential decrease of the air density ρ. The perturbation v of the particle velocity induced by wave propagation grows exponentially with the altitude. Reaching the ionosphere, the generated acoustic-gravity wave strongly affects the plasma density and plasma velocity becoming easily detectable by ionospheric monitoring.

The remarkable work of *Tanaka et al.* [1984] focused on the seismic event of Urakawa-Oki (21 March 1982, $M\omega$ 7.1): authors compared the signal of seismometers and Doppler sounders, both located in Japan. The spectral analysis of the two kinds of instruments clearly showed that the seismic signal with frequencies higher that the Brunt Väisaäilaä frequency is transferred in the atmosphere/ionosphere and detected by Doppler sounders.

Similar Doppler sounder observations of the 1968 Tokachi-Oki event ($M\omega$ 7.5) and the 1969 Kurile Island event ($M\omega$ 7.9) were presented by *Najita and Yuen* [1979]. Authors supported theoretically the hypothesis that Rayleigh waves produce only acoustic waves in the overlying atmosphere/ionosphere, and they reproduced the dispersion curve of the Rayleigh wave [*Olivier*, 1962] using Doppler sounder observations. This is the first time AQ2 that lithospheric properties are measured observing ionosphere.

Today, $AW_{Rayleigh}$ are routinely detected by Doppler sounders for events with a magnitude larger than 6.5 [*Artru et al.*, 2004]. Additionally, *Occhipinti et al.* [2010] clearly proved that over-the-horizon (OTH) radars also are able to detect the ionospheric signature of Rayleigh waves with the same sensitivity as Doppler sounders (Figure 9.2).

9.3. THE GPS REVOLUTION: FROM POINT MEASUREMENTS TO IMAGES

The advent of global positioning system (GPS) and its ability to measure the total electron content (TEC) [*Manucci et al.*, 1993, 1998] introduced a new and revolutionary tool to sound the ionosphere: the TEC is the ionospheric electron density integrated along the ray-path between receivers and satellites. As the density of the ionospheric plasma is strongly peaked, the TEC measurements are usually located at the altitude of maximum electron density, that is, at around 300 km. TEC is expressed in TEC units (TECU); 1 TECU = $10^{16} e^{-}/m^2$.

A series of exploratory works found that the TEC measured by GPS receivers was able to reveal ionospheric perturbations induced by blast explosions [*Calais et al.*, 1998], shuttle launches [*Calais and Minster*, 1996], and, of particular interest here, earthquakes [*Calais and Minster*, 1995].

The following TEC measurements, performed with dense GPS arrays, allow one to visualize the signature of Rayleigh waves in the ionosphere. In essence, the plasma perturbation detected previously in a single point by Doppler sounders is now imaged in two dimensions. Using the dense californian GPS array, *Ducic et al.* [2003] imaged for the first time the propagation of $AW_{Rayleigh}$ generated by the Alaska earthquake (3 November 2002, M_ω 7.9). The estimation of the propagation speed of Rayleigh waves from the ionospheric measurement revealed a group velocity of 3.48 km/s, in accord with seismological studies [*Larson and Ekstrom*, 2001].

Similar observations were performed in Japan with the world's densest GPS array: GEONET [*Heki and Ping*, 2005]. Authors analyzed the TEC perturbations appearing close to the epicenter after the Tokachi-Oki earthquake (25 September 2003, M_ω 8.0) and after the Southeast Off-Kii-Peninsula earthquake (5 September 2004, M_ω 6.9). This last work highlighted for the first time the difference between AGW_{epi} and $AW_{Rayleigh}$, but authors interpreted both as acoustic waves, neglecting the gravity component of the AGW_{epi}. Additionally, *Heki and Ping* [2005] observed for the first time the north/south heterogeneity induced by the magnetic field inclination. This effect plays an important role in the coupling between the neutral atmosphere and the ionospheric plasma. In essence, the postseismic TEC perturbations are amplified more when they propagate southward than when they propagate northward. Later, the effect of the magnetic field was clearly explained, matching together TEC observations and normal-mode modeling, by *Rolland et al.* [2011a] in the case of $AW_{Rayleigh}$ generated by the 12 May 2008 Wenchuan earthquake (M_ω 7.9) and by the 25 September 2003 Tokachi-Oki earthquake (M_ω 8.3).

At the present time, the postseismic TEC perturbations are routinely detected. Nevertheless, the integrated nature of TEC limits the detection to events with magnitude larger than 7.

9.4. THE GREAT SUMATRA TSUNAMI IN THE IONOSPHERE

The indirect tsunami observation by ionospheric sounding slowly followed the ionospheric detection of Rayleigh waves, mainly because of observational difficulties. The idea that tsunamis produce internal gravity waves (IGW_{tsuna}) in the atmosphere, that are detectable

by ionospheric sounding, was theoretically anticipated by *Hines* [1972] and *Peltier and Hines* [1976]. During the upward propagation, the IGW_{tsuna} is strongly amplified by the effect of the exponential decrease of the air density. The interaction of the IGW_{tsuna} with the ionospheric plasma environment produces strong variations in the plasma velocity and plasma density observable by ionospheric sounding, exactly as $AW_{Rayleigh}$ and AGW_{epi} described above (Figure 9.1).

The first observational work trying to detect the IGW_{tsuna} by ionospheric sounding was presented by *Artru et al.* [2005]. Authors measured TEC perturbations with the Japanese dense GPS network GEONET. The observed IGW_{tsuna} was supposed to be related to the Peruvian tsunamigenic quake on 23 June 2001 ($M\omega$ 8.4).

In essence, *Artru et al.* [2005] showed ionospheric traveling waves reaching the Japanese coast 22 hours after the tsunami generation, with an azimuth and arrival time consistent with tsunami propagation. Moreover, a period between 22 and 33 min, consistent with the tsunami, was identified in the observed TEC signals. The IGW_{tsuna} was, however, superimposed by other signals associated to traveling ionospheric disturbances (TIDs) [*Aframovich et al.*, 2003; *Balthazor and Moffett*, 1997]. The ionospheric noise is large in the gravity domain [*Garcia et al.*, 2005], consequently, the identification of the tsunami signature in the TEC was ambiguous.

The giant tsunami following the Sumatra-Andaman seismic event (26 December 2004, M_ω 9.3 [*Lay et al.*, 2005]), one order of magnitude larger than the Peruvian tsunami, provided worldwide remote sensing observations in the ionosphere, and provided the opportunity to explore ionospheric tsunami detection with a vast dataset. In addition to seismic waves detected by global seismic networks [*Park et al.*, 2005], coseismic displacement measured by GPS [*Vigny et al.*, 2005], oceanic sea surface variations measured by altimetry [*Smith et al.*, 2005], detection of magnetic anomaly [*Iyemori et al.*, 2005; *Balasis and Mandea*, 2007] and acoustic-gravity waves [*Le Pichon et al.*, 2005], a series of ionospheric disturbances, observed with different techniques, have been reported in the literature [*Liu et al.*, 2006a, b; *DasGupta et al.*, 2006; *Occhipinti et al.*, 2006, 2008b, 2013].

Two ionospheric anomalies in the plasma velocities were detected north of the epicenter by a Doppler sounding network in Taiwan [*Liu et al.*, 2006a]. The first was triggered by the vertical displacement induced by Rayleigh waves ($AW_{Rayleigh}$). The second, arriving one hour later with a longer period, is interpreted by *Liu et al.* [2006a] as the response of ionospheric plasma to the atmospheric gravity waves generated at the epicenter (AGW_{epi}).

AQ4 A similar long-period perturbation, with an amplitude of 4 TECU peak to peak, was observed by GPS stations located on the coast of India [*DasGupta et al.*, 2006]. Authors didn't discriminate the origin of the observed TEC perturbation, highlighting both possibilities: the IGW_{tsuna} and the AGW_{epi}. Comparable TEC observations were done for 5 GPS stations (12 station-satellite pairs) scattered in the Indian Ocean [*Liu et al.*, 2006b]. The observed amplitude was comparable to the TEC perturbations observed by *DasGupta et al.* [2006], but the propagation speed observed in the middle of the Indian Ocean by *Liu et al.* [2006b] was clearly matched by the DART AQ5 measurements of the tsunami arrival time, showing that the ionospheric perturbation and the tsunami were following each other. This result strongly supported the IGW_{tsuna} hypothesis.

Close to those observations, the Topex/Poseidon and Jason-1 satellites acquired the key observations of the Sumatra tsunami. The measured sea level displacement observed by the two altimeters was well explained by tsunami propagation models with realistic bathymetry, and provided useful constraints on source mechanism inversions [e.g., *Song et al.*, 2005]. In addition, the inferred TEC data, required to remove the ionospheric effects from the altimetric measurements [*Bilitza et al.*, 1996], showed strong ionospheric anomalies [*Occhipinti et al.*, 2006].

In essence altimetric data from Topex/Poseidon and Jason-1 showed at the same time the tsunami signature on the sea surface and the supposed tsunami signature in the ionosphere. Using a three-dimensional numerical modeling, *Occhipinti et al.* [2006] computed the atmospheric IGW_{tsuna} generated by the Sumatra tsunami as well as the interaction of the IGW_{tsuna} with the ionospheric plasma. The quantitative approach reproduced the TEC observed by Topex/Poseidon and Jason-1 in the Indian Ocean on 26 December 2004. Those observations, supported by modeling, clearly explained the nature and the existence of the tsunami signature in the ionosphere. Later, the results obtained by *Occhipinti et al.* [2006] were reproduced by *Mai and Kiang* [2009]. Other theoretical works followed *Occhipinti et al.* [2006] to calculate the effect of dissipation, nominally viscosity and thermal conduction, on the IGW_{tsuna} [*Hickey et al.*, 2009]. Additional works theoretically explored the detection capability of IGW_{tsuna} by airglow monitoring [*Hickey et al.*, 2010] and over-the-horizon radar [*Coïsson et al.*, 2011].

The method developed by *Occhipinti et al.* [2006] was also used to estimate the role of the geomagnetic field in the tsunami signature at the E-region and F-region [*Occhipinti et al.*, 2008a]. Nominally, the authors showed that the amplification of the electron density perturbation in the ionospheric plasma at the F-region is strongly dependent on the geomagnetic field inclination. This effect is explained by the Lorenz force term in the momentum equation, characterizing the neutral plasma coupling

(equation 8 in *Occhipinti et al.* [2008a]). Consequently, the detection of tsunamigenic perturbation in the F-region plasma is more easily observed at equatorial and midlatitude than at the high latitude. The heterogeneous amplification driven by the magnetic field is not observable in the E- region, consequently, detection at low altitude by HF sounding (i.e., Doppler sounding and OTH radar) is not affected by the geographical location.

Recent studies have shown the ionospheric detection of several tsunamis (Kuril, 2006, $M\omega$ 8.3; Samoa, 2009, $M\omega$ 8.1; Chile, 2010, $M\omega$ 8.8) in far field by GPS-derived TEC [*Rolland et al.*, 2010], generalizing the ionospheric detection of IGW_{tsuna} for events with lower magnitude ($M\omega \approx 8$) compared to the Sumatra event. The observed tsunami-related ionospheric perturbations, detected by the Hawaiian GPS network, appeared in the ionosphere overlying the ocean, and followed the propagation of the tsunamis at the sea level. Comparison with oceanic DART data showed similarity in the waveform as well as in the spectral signature of the ionospheric and oceanic data. This result proved again that ionosphere is a sensitive medium for tsunami propagation.

9.5. THE TOHOKU EARTHQUAKE AND TSUNAMI

9.5.1. In the Near Field

Particular attention has been paid recently to the Tohoku-Oki event (11 March 2011, $M\omega$ 9.0 [*Wei et al.*, 2012]). Thanks to the really dense GPS network in Japan (GEONET), the coseismic TEC perturbations observed at the source gave a clear image of the ionospheric perturbation in the near field [*Tsugawa el al.*, 2011; *Saito et al.*, 2011; *Rolland et al.*, 2011b], including the acoustic-gravity wave (AGW_{epi}) generated by the vertical displacement of the source [*Astafyeva et al.*, 2011, 2013], the acoustic waves coupled with Rayleigh waves ($AW_{Rayleigh}$), as well as the gravity wave induced by the tsunami propagation (IGW_{tsuna}) [*Liu et al.*, 2011; *Galvan et al.*, 2012]. The analysis of the first arrival in the TEC data in the epicentral area also allowed the localization of the epicenter with a discrepancy of less than 100 km from the official USGS location [*Tsugawa el al.*, 2011; *Tsai et al.*, 2011; *Astafyeva et al.*, 2011, 2013].

The remarkable result of *Astafyeva et al.* [2011, 2013] clearly showed that the ionospheric perturbation at the epicenter (AGW_{epi}) appears only 8 min after the rupture and shows the horizontal extension of the source. This result clearly opens the potential application of ionospheric seismology for a tsunami warning system. Indeed, the horizontal extent of the source is key information for early estimation of the tsunami amplitude.

Additionally, qualitative perturbation was also observed by four ionosondes [*Liu and Sun*, 2011] and by the Japanese SuperDARN Hokkaido radar [*Nishitami et al.*, 2011], which showed detection of the ionospheric signature of the Rayleigh waves, already observed in the past by the French OTH radar Nostradamus [*Occhipinti et al.*, 2010].

Notwithstanding the huge amount of GPS data and the clear image of the TEC perturbations at the epicentral area, discrimination between acoustic-gravity waves (AGW_{epi}) generated at the epicenter by the direct vertical displacement of the source- rupture and the internal gravity wave coupled with the tsunami (IGW_{tsuna}) was still difficult. The specific horizontal high speed of Rayleigh waves (≈3.5 km/s) separates and makes really recognizable the $AW_{Rayleigh}$ in the ionosphere.

The recent work of *Occhipinti et al.* [2013] collects ionospheric TEC data from several ground networks in order to visualize and analyze the ionospheric perturbations at the epicenter of the following events: Sumatra, 26 December 2004, $M\omega$ 9.1, and 12 September 2007, $M\omega$ 8.5; Chile, 14 November 2007, $M\omega$ 7.7; Samoa, 29 September 2009, $M\omega$ 8.1; and the catastrophic Tohoku-Oki event, 11 March 2011, $M\omega$ 9.0 (Figure 9.3). The work introduces some theoretical bases to interpret the data and discriminate between AGW_{epi} and IGW_{tsuna}. Section 6 summarizes the physical properties of the different waves described.

9.5.2. In the Far Field

Far away from the epicentral area, the AGW_{epi} generated by the direct vertical displacement of the ground and directly linked to the rupture are strongly attenuated and not detectable anymore by ionospheric sounding. In the far field, the propagation of $AW_{Rayleigh}$ and IGW_{tsuna} is completely separated as a consequence of the tremendous difference of horizontal speed of Rayleigh waves (≈3.5 km/s) and tsunamis (≈200 m/s). This is the main reason why, as described above, the $AW_{Rayleigh}$ and IGW_{tsuna} have been already detected by ionospheric sounding by different techniques. Notwithstanding that the $AW_{Rayleigh}$ and IGW_{tsuna} are today routinely detected in the far field, the Tohoku event observations opened new perspectives in ionospheric seismology.

First of all, the $AW_{Rayleigh}$ and IGW_{tsuna} were detected initially in the neutral atmosphere instead of the ionosphere [*Garcia et al.*, 2013, 2014]. The gravity mission GOCE crossed the wave front of $AW_{Rayleigh}$ [*Garcia et al.*, 2013] and IGW_{tsuna} [*Garcia et al.*, 2014] measuring the airspeed variation and the air-density variation. Those measurements represent a useful benchmark to validate the propagation modeling of $AW_{Rayleigh}$ and IGW_{tsuna} in the neutral atmosphere, and, combined with ionospheric observations, additionally allow one to explore the physics of the neutral-plasma coupling. AQ6

Second, the detection of IGW_{tsuna} by airglow, mentioned before, has been recently validated by observation [*Makela et al.*, 2011] and modeling [*Occhipinti et al.*, 2011] in the case of the Tohoku event (11 March 2011, M_ω 9.0). The airglow is measuring the photon emission at 630 nm, indirectly linked to the plasma density of O^+ [*Link and Cogger*, 1988] and it is commonly used to detect transient events in the ionosphere [*Kelley et al.*, 2002; *Makela et al.*, 2009; *Miller et al.*, 2009]. The modeling of the IGW_{tsuna} clearly reproduced the pattern of the airglow measurement observed over Hawaii (Figure 9.4). The comparison between the observation and the modeling

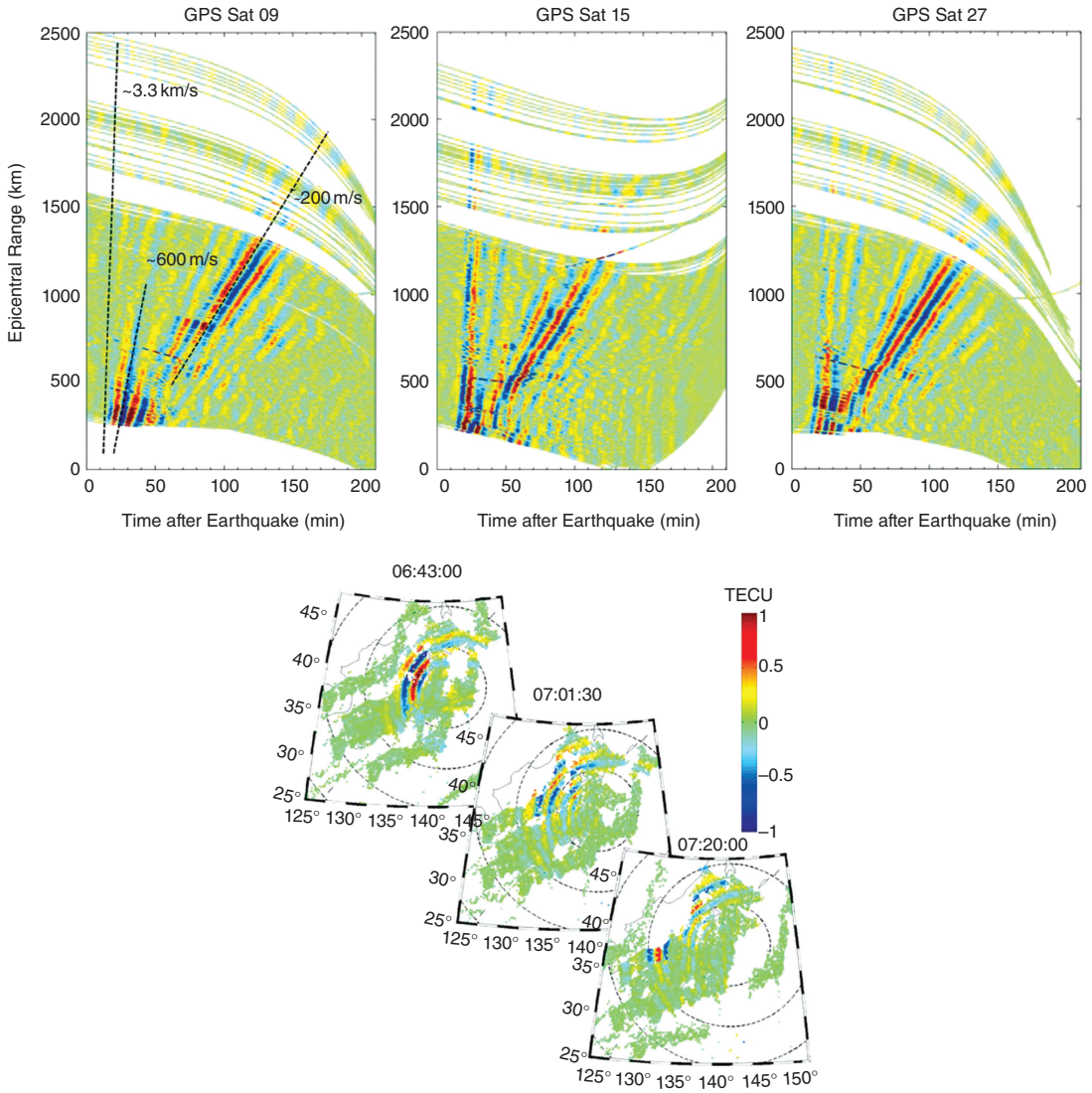

Figure 9.3 Hodochrones (left) of the TEC perturbation observed by the Japanese GEONET network and by eight satellites (indicated in the top) following the recent Tohoku-Oki tsunamigenic earthquake (2011, M: 9.0). We observe $AW_{Rayleigh}$ with a speed of around 3.3 km/s, AGW_{epi} moving with a speed of around 650 m/s. The AGW_{epi} disappears after 500–1000 km, and it is replaced by IGW_{tsuna} with a speed of around 200 m/s. (Adapted from *Occhipinti et al.* [2013].) On the right, the data are represented over Japan using all satellites. (Adapted from *Rolland et al.* [2011b].)

AQ8

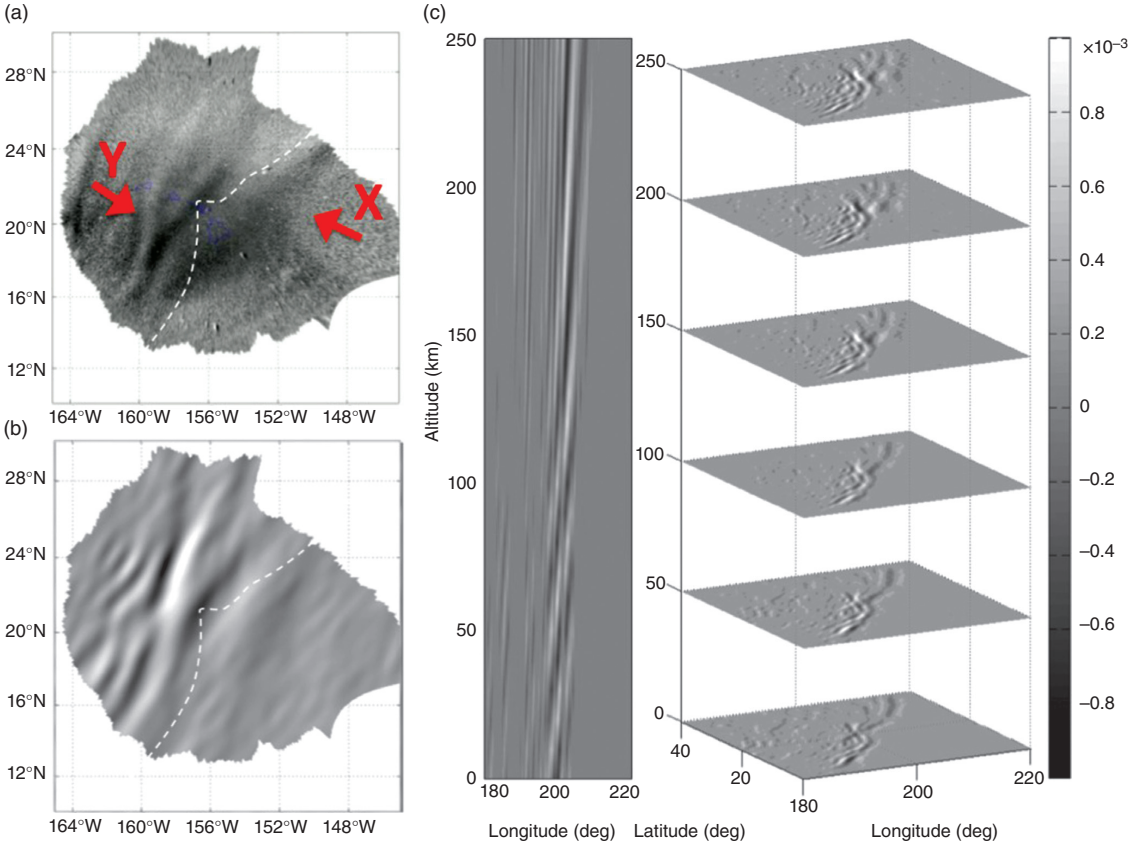

Figure 9.4 Airglow perturbation of the IGW_{tsuna} (a) observed by the camera located in Hawaii during the Tohoku tsunami (2011), and (b) the modeling of the IGW_{tsuna} for the layer corresponding to the observation, and (c) the entire structurein 3D. (Adapted from *Occhipinti et al.* [2011].)

allows one to recognize not only the evident Y shape, but also the longer wavelength perturbation (indicated with X in Figure 9.4) that arrives before the tsunami wavefront by the effect of bathymetry [*Occhipinti et al.*, 2011]. Approaching the Hawaiian archipelago, the tsunami propagation is slowed down (reduction of the sea depth), but, the IGW_{tsuna}, propagating in the atmosphere/ionosphere, conserves its speed.

An additional measurement following the Queen Charlotte event (27 October 2012, M_ω 7.8) has been recently detected, proving that the technique can be generalized for smaller events [Makela, 2012]. In order to deeply explore the detection by airglow, four cameras were recently installed in Chile, Hawaii, and Tahiti in order to detect the signature of future tsunamis.

AQ7

The potential echo of the detection of IGW_{tsuna} by airglow, using ground-based or on-board cameras, could change the future of tsunami detection and warning systems.

9.6. PHYSICAL PROPERTIES OF $AW_{Rayleigh}$, IGW_{tsuna}, AND AGW_{epi}

The physical properties of the three components can be summarized as follow: The $AW_{Rayleigh}$, clearly observed in the far field, has a horizontal speed of ≈3.5 km/s imposed by the forcing source, nominally the Rayleigh wave. The $AW_{Rayleigh}$ has two main frequencies of 3.68 mHz and 4.44 mHz, corresponding to the coupled normal modes ${}_0S_{29}$ and ${}_0S_{37}$, respectively. Consequently, as the propagating wave is an acoustic wave, the vertical velocity of $AW_{Rayleigh}$ is close to the acoustic wave speed, and the corresponding time to reach the ionospheric layers is on the order of 8–15 min (Figure 9.5). Additional frequencies around those major peaks, with small amplitudes, have been observed in the past by *Najita and Yuen* [1979] using Doppler sounders and recently by *Bourdillon et al.* [2014] using OTH radar. Additional spectral analysis of the

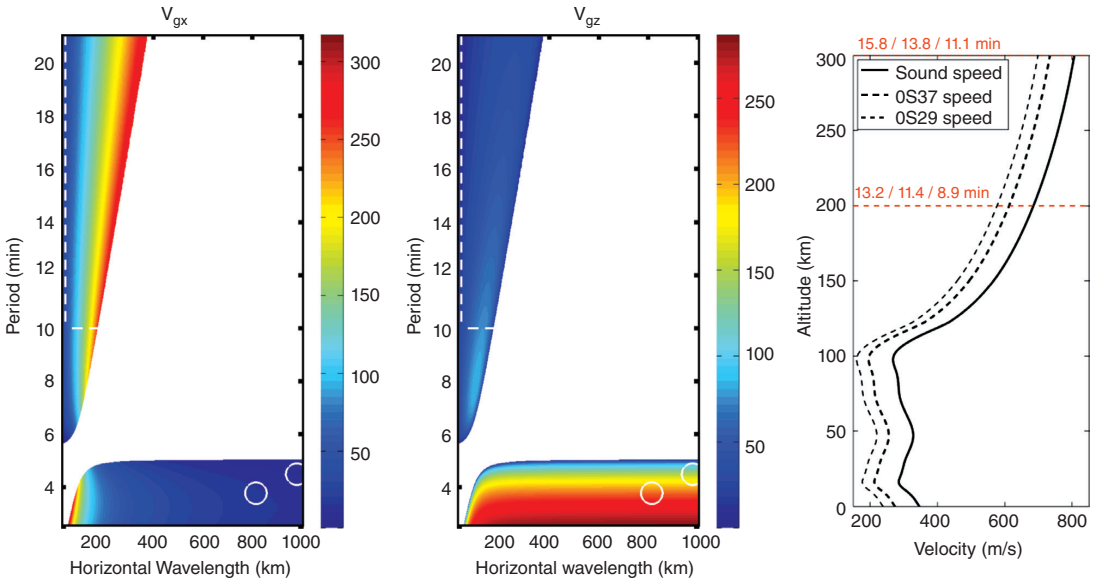

Figure 9.5 (Left) Horizontal and (center) vertical group velocity at the atmospheric bottom boundary, computed following *Watada* [2009]. The white dotted line limits the λ/T region of IGW_{tsuna}; the two white circles highlight the position of Rayleigh waves linked to ${}_0S_{29}$ and ${}_0S_{37}$. (Right)Supposing that the vertical evolution of the speed follows the sound speed, the vertical group velocity of ${}_0S_{29}$ and ${}_0S_{37}$ is compared with the sound speed, and the propagation time to reach 200mkm and 300 km of altitude is highlighted in red.

signal observed by *Occhipinti et al.* [2010] by Doppler sounder and OTH radar is computed here (Figure 9.2), and clearly shows that the Rayleigh wave signature is still visible at higher frequency (until 50 mHz). Comparison between data and modeling by normal mode summation [*Artru et al.*, 2004; *Occhipinti et al.*, 2010] for a complete stratified 1D Earth with solid and fluid (ocean and atmosphere) parts, clearly proved that our description of $AW_{Rayleigh}$ is satisfying enough (Figure 9.2) for using ionospheric data for magnitude estimation, source localization, as well as moment tensor inversion. Indeed, as showed by Figure 9.2, the amplitude of the main phase is well described by the modeling. At the higher frequencies, the effect of the lithospheric heterogeneity is not reproduced by the modeling showing the limit of the normal mode summation for 1D Earth.

The IGW_{tsuna}, clearly observable in the far field, has horizontal and vertical speeds that are clearly defined by *Occhipinti et al.* [2013] and depending of the physical properties of the tsunami:

$$v_g^h = \frac{k_h N^2 \left(D - k_h^2\right)}{\omega D^2} \qquad v_g^z = \frac{k_z k_h^2 N^2}{\omega D^2}$$

where k_z and k_h are the vertical and horizontal $k-$vectors, ω the frequency of the tsunami, N is the Brunt Väisaäilaä frequency, and $D = k_z^2 + k_h^2 + \left(\frac{N^2}{2g}\right)^2$. Please, note that the vertical group velocity v_g^z has an opposite sign compared to the vertical phase velocity (ω/k_z). This is a typical propagation characteristic of internal gravity waves: the atmosphere falls down by the effect of the gravity, and consequently the vertical phase velocity is negative while the vertical group velocity is positive, generating the upward propagation of the IGW_{tsuna}. The vertical group velocity v_g^zallows to compute the propagation time delay to reach the ionospheric layers (Figure 9.6). AQ9

The horizontal phase velocity of the IGW_{tsuna} is the same as the tsunami $\left(\omega/k_h = v_{tsuna} = \sqrt{gH}\right)$. However, this is no longer the case for the horizontal group velocity v_g^z, which is furthermore dispersive. In the case of tsunami, the group and phase velocities are the same. The horizontal group velocity of the generated IGW_{tsuna} is always smaller than the horizontal phase velocity (Figure 9.6).

The horizontal group velocity v_g^h does not play a role in the vertical propagation delay but it is useful to estimate the epicentral distance where the IGW_{tsuna} starts to interact with the ionosphere, and it is also useful to estimate the delay δt between the tsunami propagating at the sea surface and the IGW_{tsuna} propagating in the atmosphere at the altitude z_{iono} (Figure 9.6). The period of a tsunami and

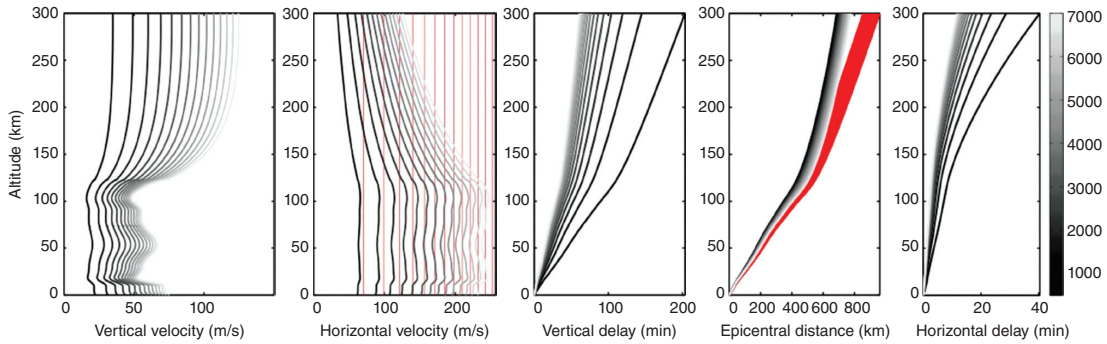

AQ11

Figure 9.6 From left to right: vertical (v_g^z) and the horizontal (v_g^h) group velocity of the IGW_{tsuna}, generated at different oceanic deep h (m), see gray scale, and a characteristic period T of 10 min. Red lines in v_g^h show the tsunami speed ($v_{tsuna} = \sqrt{hg}$, where g is the gravity acceleration). Consequent vertical propagation delay (third from left); epicentral distances covered by the tsunami (red) and the coupled IGW (gray scale) during the delay spent by the IGW_{tsuna} to reach the altitude shown in the y-axis (fourth from left); last on the right: horizontal delay $\ddot{a}t$ between the tsunami at sea level and the coupled IGW_{tsuna} at fixed altitudes (time to cross the same zenith). (Adapted from *Occhipinti et al.* [2013].)

the consequent IGW_{tsuna} is generally between 10 min and 40 min. As the group velocity depends on ω, the period variation (10–40 min) introduces strong variation in the vertical propagation delay (60–240 min to reach, e.g., 200 km of altitude), the epicentral distance (500–2500 km), as well as the delay δt (8–2 min) [*Occhipinti et al.*, 2013].

AQ10

The AGW_{epi} is the more complex part of the signal observed in the ionosphere. The rupture and the consequent ground displacement at the source area has a rich spectral signature: consequently, both acoustic and gravity waves are simultaneously generated. The preliminary work of *Matsumura et al.* [2011] partially reproduce, by a 2D numerical modeling, some of the observed AGW_{epi}. Anyway, until now, no exhaustive modeling of the ionospheric perturbations at the epicentral area has been performed. Based on the interesting theoretical work of *Watada* [2009], about the acoustic-gravity wave properties at the bottom boundary of the atmosphere, it is possible to generalize the horizontal and vertical speed of the AGW_{epi} at the surface/atmosphere boundary:

$$boundary\ v_g^h = \frac{c_s^2 \omega}{\omega^4 - k_h^2 N^2 c_s^2} k_h \left(\omega^2 - N^2\right)$$

$$boundary\ v_g^z = \frac{c_s^2 \omega}{\omega^4 - k_h^2 N^2 c_s^2} k_z \omega^2$$

where c_s, in addition to the notation described above, is speed of the sound. Again, to avoid misunderstanding, *Watada* [2009] describes a formalism in an isothermal atmosphere to compute group speed of AGW_{epi}. Consequently, the $_{boundary}\,\mathbf{v}_g$ is valid only at the surface/atmosphere boundary. In the λ/T region describing tsunamis, the values of $_{boundary}\,\mathbf{v}_g$ are consistent with the values of $\mathbf{v}_g$ computed at the surface/atmosphere boundary (Figure 9.5). Figure 9.5 clearly shows the inversion of vertical and horizontal group velocity for acoustic and gravity waves. The $AW_{Rayleigh}$ has a vertical speed slightly slower than the sound speed, consequently it takes around 10–15 min to reach the ionosphere. Consistent with the formalism described above [*Occhipinti et al.*, 2013], IGW_{tsuna} needs 1–2 hours to reach the ionosphere. The AGW_{epi}, generated by the vertical ground displacement at the epicenter, contains a more high-frequency component (0.5–1 Hz) that is transferred to the atmosphere with the sound speed c_s. Consequently, the high-frequency component of AGW_{epi} appears in the ionosphere in around 8 min, as observed by *Astafyeva et al.* [2011, 2013].

I wish to highlight again that today no numerical methods are able to fully describe the AGW_{epi}. Indeed, the work of *Matsumura et al.* [2011] is limited to the 2D neutral atmosphere and partially reproduces the observed waves. The normal mode summation for a complete planet [*Lognonné et al.*, 1998] has been used only to explain the $AW_{Rayleigh}$, and emphasized the limit of a 1D model. As shown in Figure 9.2, the synthetics strictly satisfy the data only for frequency under 10 mHz; higher frequencies are more sensitive to the heterogeneities of the upper crust and need 3D modeling. An appropriate method could be the spectral element method (SEM) usually applied for seismology with excellent results [e.g., *Komatitsch and Tromp*, 2002]. One quick test with SEM clearly shows that the methodology can easily take into account the propagation of acoustic waves (Figure 9.7),

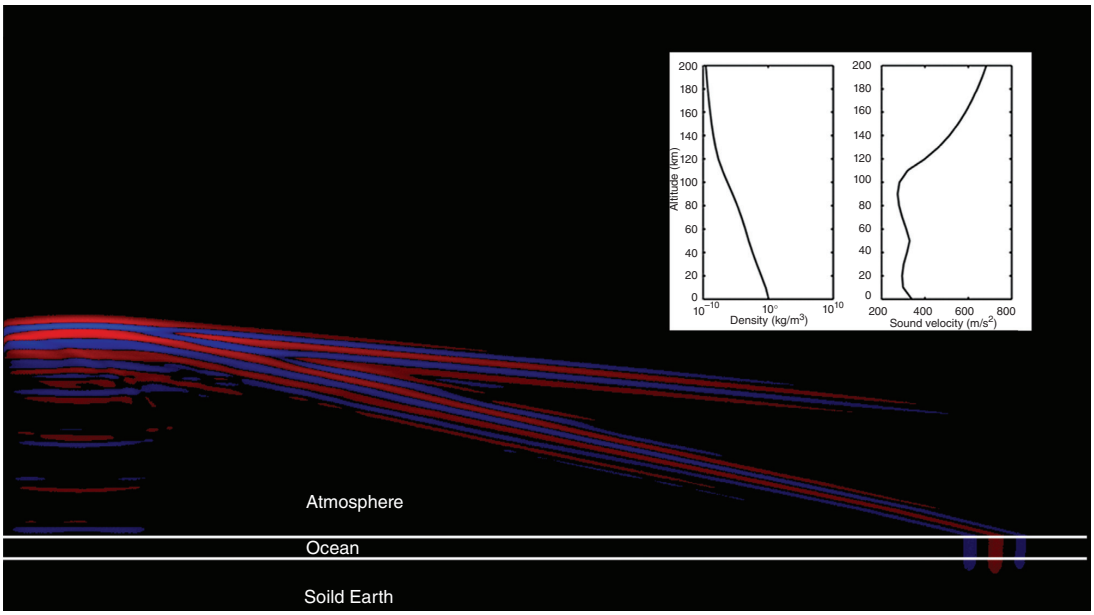

Figure 9.7 Propagation of seismic and acoustic waves in the solid Earth crust (20 km, $\rho = 2.5\ kg/m^3$, $V_p = 3.4\ km/s$, $V_s = 1.96\ km/s$), ocean (10 km, $\rho = 1.02\ kg/m^3$, $V_p = 1.45\ km/s$, $V_s = 0.0\ km/s$), and atmosphere (200 km, ρ, and sound speed in the inset) modeled by SPECFEM2D [e.g., *Komatitsch* and *Tromp,* 2002]. The propagation of Rayleigh wave in the solid part is transferred quickly to the ocean, then into the atmosphere. We also see the signature in the atmosphere of the P-waves, their amplitude becomes smaller when we are far away from the source, compared to Rayleigh wave signature.

but the propagation of gravity waves and tsunamis is not implemented yet in the SEM. In the other side, the method developed by *Occhipinti et al.* [2006, 2008a, 2013], even if it is totally 3D, propagates only gravity waves and is able to reproduce only the IGW_{tsuna} plus the gravity component of AGW_{epi}. One of the objectives of this work is to push forward the theoretical development of the propagation of acoustic-gravity waves coupled with the vertical displacement of the ground and ocean, in order to completely reproduce the AGW_{epi}. The full understanding and the dense measurement of AGW_{epi} is a key step for future tsunami warning systems.

9.7. CONCLUSION

The fact that humans don't fly is the main reason why seismology studied only solid Earth. If humans were Hawk Men of the gravitating city of Mongo [*Raymond*, 1934], they would know from the beginning that earthquakes and tsunamis disturb the upper fluid envelope, mainly atmosphere/ionosphere.

This work traces the evolution of the idea of the unique planet, where the solid Earth, the ocean, as well as the atmosphere/ionosphere continuously exchange energy, with particular emphasis during natural hazards like earthquakes; volcanic or, more generally, atmospheric explosions; and tsunamis.

On the basis of theoretical considerations and observational proofs, the natural hazard signatures in the ionosphere are classified here following the source and physical characteristic of the generated waves: the AGW_{epi} is the acoustic-gravity wave generated by rupture and observable at the epicentral area within the first 1000 km; the $AW_{Rayleigh}$ is the acoustic wave generated by propagation of Rayleigh wave; and the IGW_{tsuna} is the internal gravity wave coupled and forced by the tsunami propagation.

Starting from the early atmospheric/ionospheric detection related to seismic events and nuclear explosions during the Cold War, this work highlights the role of Doppler sounders and OTH radar as ionospheric seismometers able to measure the $AW_{Rayleigh}$ (and consequently the lithospheric properties intrinsic in the Rayleigh wave propagation) sounding ionosphere at 200 km of altitude. This work also highlights the capability of GPS, measuring the total electron content (TEC), to image the propagation of the atmospheric/ionospheric signature of the AGW_{epi}, the $AW_{Rayleigh}$, and the IGW_{tsuna}.

The recent Tohoku event in Japan generated a tremendous earthquake and a consequent tsunami. The event generated catastrophic consequences, but the huge amount of collected data strongly helps the earthquake science evolution. The ionosphere sounded by the world's densest GPS network GEONET showed a clear image of the rupture extent observing the AGW_{epi} propagating in the atmosphere/ionosphere overlying Japan (including the epicentral area and the oceanic regions). In the far field, the airglow camera located in Hawaii showed without doubt the IGW_{tsuna} propagation over a region of $180\times180\,km^2$ in the ionosphere overlying the islands. Never before was a tsunami measured off shore with such high spatial resolution.

Unfortunately, the estimation of the ground and sea surface displacement via ionospheric sounding is still not a direct measurement. Indeed, the ionospheric perturbation is modulated by the magnetic field inclination, and, even if this effect could be controlled by some a priori information, the integrated nature of TEC measured by GPS imposes the solution of an inverse problem to estimate the tsunami amplitude at sea level. Consequently, the measurement, the full understanding, and the accurate quantitative modeling of AGW_{epi}, $AW_{Rayleigh}$, and IGW_{tsuna} are necessary steps to fruitfully use ionospheric monitoring to prevent disasters.

The monitoring by dense GPS networks of the ionosphere overlying the subduction zones could greatly help the estimation of the source extent. Future satellites with on-board airglow cameras could track tsunami propagation over entire oceans before they hit the coast.

With this work I wish to encourage the use of ionospheric seismology as a potential support for future earthquake and tsunami warning systems.

ACKNOWLEDGMENT

This project is supported by the Programme National de Télédétection Spatiale (PNTS), grant n PNTS-2014-07, by the CNES grant SI- EuroTOMO and by the ONR project TWIST. I thanks J.-P. Avouac (Caltech Tectonic Observatory), Jeroen Tromp (Princeton), Claudio Satriano (Institut de Physique du Globe de Paris), and Shingo Watada (Earthquake Research Institute) for friendly and constructive suggestions. I thank A. De Santis and two anonymous reviewers for their constructive remarks. This is IPGP contribution 3573.

REFERENCES

Aframovich, E. L., N. P. Perevalova, and S. V. Voyeikov (2003), Traveling wave packets of total elctron content disturbances as deduced from GPS network data, *J. Atmo. Solar-Terr. Phys.*, *65*, 1245–1262.

AQ12 Aristoteles (524), *Meteorologia Aristotelis*, Book II.

Artru, J., T. Farges, and P. Lognonné (2004), Acoustic waves generated from seismic surface waves: Propagation properties determined from Doppler sounding and normal-mode modeling, *Geophys. J. Int.*, *158*(3), 1067–1077.

Artru, J., V. Ducic, H. Kanamori, P. Lognonné, and M. Murakami (2005), Ionospheric detection of gravity waves induced by tsunamis, *J. Geophys. Res.*, *160*, 840.

Astafyeva, E., L. Rolland, P. Lognonne, K. Khelfi, and T. Yahagi (2013), Parameters of seismic source as deduced from 1 Hz ionospheric GPS data: Case study of the 2011 Tohokuoki event, *J. Geophys. Res. Space Physics*, *118*, 59425950, doi:10.1002/jgra.50556.

Astafyeva, E., P. Lognonné, and L. Rolland (2011), First ionosphere images for the seismic slip of the Tohokuoki earthquake, *Geophys. Res. Lett.*, doi:10.1029/2011GL049623.

Balasis G., and M. Mandea (2007), Can electromagnetic disturbances related to the recent great earthquakes be detected by satellite magnetometers? *Special issue Mechanical and Electromagnetic Phenomena Accompanying Preseismic Deformation: From Laboratory to Geophysical Scale*, ed. by K. Eftaxias, T. Chelidze, and V. Sgrigna, *Tectonophysics*, *431*, doi:10.1016/j.tecto.2006.05.038.

Balthazor, R. L., and R. J. Moffett (1997), A study of atmospheric gravity waves and travelling ionospheric disturbances at equatorial latitudes, *Ann. Geophysicae*, *15*, 1048–1056.

Bilitza, D., C. Koblinsky, S. Zia, R. Williamson, and B. Beckley (1996), The equator anomaly region as seen by the TOPEX/Poseidon satellite, *Adv. Space Res.*, *18*, 6, 23–32.

Bolt, B. A. (1964), Seismic air waves from the great 1964 Alaskan earthquake, *Nature* (June 13). AQ13

Bourdillon, A., G. Occhipinti, J.-P. Molinié, and V. Rannou (2014), HF radar detection of infrasonic waves generated in the ionosphere by the 28 March 2005 Sumatra earthquake, *J. Atmo. Solar-Terr. Phys.*, *109* (March), 75–79, doi:10.1016/j.jastp.2014.01.008.

Calais, E., and J. B. Minster (1995), GPS detection of ionospheric perturbations following the January, 1994, Northridge earthquake, *Geophys. Res. Lett.*, *22*(9), 1045–48.

Calais, E., and J. B. Minster(1996), GPS detection of ionospheric perturbations following a Space Shuttle ascent, *Geophys. Res. Lett.*, *23*, 15, 1897–1900.

Calais, E., J. B. Minster, M. A. Hofton, and M. A. H. Hedlin (1998), Ionospheric signature of surface mine blasts from Global Positioning System measurement, *Geophys. J. Int.*, *132*,191–202.

Coïsson, P., G. Occhipinti, P. Lognonné, and L. M. Rolland (2011), Tsunami signature in the ionosphere:the innovative role of OTH radar, *Radio Sci.*, *46*, RS0D20, doi:10.1029/2010RS004603.

DasGupta, A., A. Das, D. Hui, K. K. Bandyopadhyay, and M. R. Sivaraman (2006), Ionospheric perturbation observed by the GPS following the December 26th, 2004 Sumatra-Andaman earthquake, *Earth Planet. Space*, *35*, 929–959.

Davies, K., and D. M. Baker, Ionospheric effects observed around the time of the Alaskan earthquake of March 28, 1964, *J. Geophys. Res.*, *70*, 2251–2253, 1965.

Donn, W., and E. S. Posmentier, Ground-coupled air waves from the great Alaskan earthquake, *J. Geophys. Res.*, *69*, 5357–5361, 1964.

Ducic, V., J. Artru, and P. Lognonné (2003), Ionospheric remote sensing of the Denali Earthquake Rayleigh surface waves, *Geophys. Res. Lett.*, *30*, 18, 1951, doi:10.1029/2003GL017812.

Galvan, D. A., A. Komjathy, M. P. Hickey, P. Stephens, J. Snively, Y. T. Song, M. D. Butala, and A. J. Mannucci

(2012), Ionospheric signatures of Tohoku-Oki tsunami of March 11, 2011: Model comparisons near the epicenter, *Radio Science*, *47*, 4003, doi 10.1029/2012RS005023.

Garcia, R., F. Crespon, V. Ducic, and P. Lognonné (2005), 3D ionospheric tomography of post-seismic perturbations produced by Denali earthquake from GPS data, *Geophys. J. Int.*, *163*, 1049–1064, doi: 10.1111/j.1365-246X.2005.02775.x.

Garcia, R. F., S. Bruinsma, P. Lognonné, E. Doornbos, and F. Cachoux (2013), GOCE: The first seismometer in orbit around the Earth, *Geophys. Res. Lett.*, *40*, doi:10.1002/grl.50205.

Garcia, R. F., E. Doornbos, S. Bruinsma, and H. Hebert (2014), Atmospheric gravity waves due to the Tohoku-Oki tsunami observed in the thermosphere by GOCE, *J. Geophys. Res. Atmos.*, *119*, doi:10.1002/2013JD021120.

Heki, K., and J. Ping (2005), Directivity and apparent velocity of the coseismic traveling ionospheric disturbances observed with a dense GPS network, *Earth Planet Sci. Lett*., *236*, 3–4, 15, 845–855.

Hickey, M. P., G. Schubert, and R. L. Walterscheid (2009), The propagation of tsunami-driven gravity waves into the thermosphere and ionosphere, *J. Geophys. Res.*, *114*, A08304, doi:10.1029/2009JA014105.

Hickey, M. P., G. Schubert, and R. L. Walterscheid (2010), Atmospheric airglow fluctuations due to a tsunami-driven gravity wave disturbance, *J. Geophys. Res.*, *115*, A06308, doi:10.1029/2009JA014977.

Hines, C.O. (1972), Gravity waves in the atmosphere, *Nature*, *239*, 73–78.

Iyemori, T., M. Nose, D. S. Han, Y. F. Gao, M. Hashizume, N. Choosakul, H. Shinagawa, Y. Tanaka, M. Utsugi, A. Saito, H. McCreadie, Y. Odagi, and F. X. Yang (2005), Geomagnetic pulsations caused by the Sumatra earthquake on December 26, 2004, *Geophys. Res. Lett*., *32*, L20807.

Kanamori, H., and J. Mori (1992), Harmonic exitation of mantle Rayleigh waves by the 1991 eruption of Mount Pinatubo, Philippines, *Geophys. Res. Lett.*, *19*, 721–724.

Kelley, M. C., J. J. Makela, B. M. Ledvina, and P. M. Kintner (2002), Observations of equatorial spread?F from Haleakala, Hawaii, *Geophys. Res. Lett.*, *29*(20), 2003, doi:10.1029/2002 GL015509.

Kobayashi, N., K. Nishida, and Y. Fukao (1998), Continuous exitation of Earth's free oscillations, *Nature*, *395*,357–360.

Komatitsch, D., and J. Tromp (2002), Spectral-element simulations of global seismic wave propagation, I Validation, *Geophys*. *J. Int.*, *149*(2), 390–412.

Larson, E. W., and G. Ekstrom (2001), Global models of surface wave group velocity, *Pure Ap*. *Geophys.*, *158*, 13771399.

Lay, T., H. Kanamori, C. J. Ammon, M. Nettles, S. N. Ward, R. C. Aster, S. L. Beck, S. L. Bilek, M. R. Brudzinski, R. Butler, H. R. DeShon, G. Ekstrom, K. Satake, and S. Sipkin (2005), The great Sumatra-Andaman earthquake of 26 December 2004, *Science*, *308*, 1127–1133.

Leonard, R. S., and R. A. Barnes, Jr (1964), Observation of ionospheric disturbances following the Alaskan earthquake, *J. Geophys. Res.*, *70*, 1250–1253.

Le Pichon, A., P. Herry, P. Mialle, J. Vergoz, N. Brachet, M. Garces, D. Drob, and L. Ceranna (2005), Infrasound associated with 2004-2005 large Sumatra earthquakes and tsunami, *Geophys. Res. Lett.*, *32*, L19802.

Link, R., and L. L. Cogger (1988), A reexamination of the O I 6300 nightglow, *J. Geophys. Res.*, *93*(A9), 98839892.

Liu, J., Y. Tsai, K. Ma, Y. Chen, H. Tsai, C. Lin, M. Kamogawa, and C. Lee (2006a), Iono– spheric GPS total electron content (TEC) disturbances triggered by the 26 December 2004 Indian Ocean tsunami, *J. Geophys. Res.*, *111*, A05303.

Liu, J. Y, Y. B. Tsai, S. W. Chen, C. P. Lee, Y. C. Chen, H. Y. Yen, W. Y. Chang, and C. Liu (2006b), Giant ionospheric distrubances excited by the M9.3 Sumatra earthquake of 26 December 2004, *Geophys. Res. Lett*., *33*, L02103.

Liu, J.-Y., and Y.-Y. Sun (2011), Seismo-traveling ionospheric disturbances of ionograms observed during the 2011 Mw 9.0 Tohoku Earthquake, *Earth Planets Space*, *63*, 897–902.

Liu, J.-Y., C.-H. Chen, C.-H. Lin, H.-F. Tsai, C.-H. Chen, and M. Kamogawa (2011), Ionospheric disturbances triggered by the 11 March 2011 M9.0 Tohoku earthquake, *J. Geophys. Res*., *116*, doi10.1029/2011JA016761.

Lognonné, P., E. Clévédé, and H. Kanamori (1998), Computation of seismograms and atmospheric oscillations by normal-mode summation for a spherical Earth model with realistic atmosphere, *Geophys. J. Int.*, *135*, 388–406.

Mai, C.-L., and J.-F. Kiang (2009), Modeling of ionospheric perturbation by 2004 Sumatra tsunami, *Radio Sci.*, *44*, RS3011, doi:10.1029/2008RS004060.

Makela, J. J., M. C. Kelley, and R. T. Tsunoda (2009), Observations of midlatitude ionospheric instabilities generating meter scale waves at the magnetic equator, *J. Geophys. Res.*, *114*, A01307, doi:10.1029/ 2007JA012946.

Makela, J. J., P. Lognonné, H. Hébert, T. Gehrels, L. Rolland, S. Allgeyer, A. Kherani, G. Occhipinti, E. Astafyeva, P. Coïsson, A. Loevenbruck, E. Clévédé, M. C. Kelley, and J. Lamouroux (2011), Imaging and modelling the ionospheric response to the 11 March 2011 Sendai Tsunami over Hawaii, *Geophys. Res. Let.*, *38*, L20807, doi:10.1029/2011GL047860.

Manucci, A. J., B. D. Wilson, and C. D. Edwards (1993), A new method for monitoring the Earth's ionospheric total electron content using GPS global network, Paper presented at *ION GPS-93*, Salt Lake City, September 22–24.

Manucci, A. J., B. D. Wilson, D. N. Yuan, C. H. Ho, U. J. Lindqwister, and T. F. Runge (1998), A global mapping technique for GPS-derived ionospheric electron content measurements, *Radio Sci.*, *33*, 565–582.

Matsumura, M., A. Saito, T. Iyemori, H. Shinagawa, T. Tsugawa, Y. Otsuka, M. Nishioka, and C. H. Chen (2011), Numerical simulations of atmospheric waves excited by the 2011 off the Pacific coast of Tohoku Earthquake, *Earth Planets Space*, *63*, 885889, doi:10.5047/eps.2011.07.015.

Miller, E. S., J. J. Makela, and M. C. Kelley (2009), Seeding of equatorial plasma depletions by polarization electric fields from middle latitudes: Experimental evidence, *Geophys. Res. Lett.*, *36*, L18105, doi:10.1029/ 2009GL039695.

Najita, K., and P. C. Yuen (1979), Long-period oceanic Rayleigh wave group velocity dispersion courve from HF doppler sounding of the ionosphere, *J. Geophys. Res.*, *84*, 1253–1260.

Nawa, K., N. Suda, Y. Fukao, T. Sato, Y. Aoyama, and K. Shibuya (1998), Incessant excitation of the earths free oscillations, *Earth Planet. Space*, *50* (38).

Nishida, K., N. Kobayashi, and Y. Fukao (2000), Resonant oscillations between the solid Earth and the atmosphere, *Science*, *287*, 2244–2246.

Nishitani, N., T. Ogawa, Y. Otsuka, K. Hosokawa, and T. Hori (2011), Propagation of large amplitude ionospheric disturbances with velocity dispersion observed by the SuperDARN Hokkaido radar after the 2011 off the Pacific coast of Tohoku Earthquake, *Earth Planets Space*, *63*, 891896.

Occhipinti, G., A. Komjathy, and P. Lognonné (2008b), Tsunami detection by GPS: How ionospheric observation might improve the Global Warning System, *GPS World*, *Feb.*, 50–56,

Occhipinti, G., E. Alam Kherani, and P. Lognonné (2008a), Geomagnetic dependence of ionospheric disturbances induced by tsunamigenic internal gravity waves, *Geophys. J. Int.*, doi: 10.1111/j.1365-246X.2008.03760.x.

Occhipinti, G., L. Rolland, P. Lognonné, and S. Watada (2013), From Sumatra 2004 to Tohoku-Oki 2011: The systematic GPS detection of the ionospheric signature induced by tsunamigenic earthquakes, *J. Geophys. Res. Space Physics*, *118*, doi:10.1002/jgra.50322.

Occhipinti, G., P. Coïsson, J. J. Makela, S. Allgeyer, A. Kherani, H. Hēbert, and P. Lognonné (2011), Three-dimensional numerical modeling of tsunami-related internal gravity waves in the Hawaiian atmosphere, submitted to *Earth Planet, Science*, *63* (7), 847–851, , doi:10.5047/eps.2011.06.051.

Occhipinti, G., P. Dorey, T. Farges, and P. Lognonné (2010), Nostradamus: The radar that wanted to be a seismometer, *Geophys. Res. Lett.*, doi:10.1029/2010GL044009.

Occhipinti, G., P. Lognonné, E. Alam Kherani, and H. Hebert (2006), Three-dimensional wave- form modeling of ionospheric signature induced by the 2004 Sumatra tsunami, *Geophys. Res. Lett.*, *33*, L20104.

Olivier, J. (1962), A summary of observed seismic surface wave dispersion, *Bull. Seismol. Soc. Amer.*, *44*, 127.

Park, J., K. Anderson, R. Aster, R. Butler, T. Lay, and D. Simpson (2005), Global Seismographic Network records the Great Sumatra-Andaman earthquake, *EOS Trans. AGU*, *86*(6), 60.

Peltier, W. R., and C. O. Hines (1976), On the possible detection of tsunamis by a monitoring of the ionosphere, *J. Geophys. Res.*, *81*,12.

AQ14 Raymond, A. (1934), Fash Gordon, King Features Syndicate.

Rhie, J., and B. Romanowicz (2004), Excitation of Earths continuous free oscillations by atmosphere-ocean-seafloor coupling, *Nature*, *431*, 552–556.

Rolland, L., G. Occhipinti, P. Lognonné, and A. Loevenbruck (2010), The 29 September 2009 Samoan tsunami in the ionosphere detected offshore Hawaii, *Geophys. Res. Lett.*, *37*, L17191 doi:10.1029/2010GL044479.

Rolland, L. M., P. Lognonné, and H. Munekane (2011a), Detection and modeling of Rayleigh waves induced patterns in the ionosphere, *J. Geophys. Res.*, *116*:A05320. DOI: 10.1029/2010JA016060.

Rolland, L. M., P. Lognonné, E. Astafyeva, E. A Kherani, N. Kobayashi, M. Mann, and H. Munekane (2011b), The resonant response of the ionosphere imaged after the 2011 off the Pacific coast of Tohoku Earthquake, *Earth Planets Space*, *63*, 853–857.

Roult, G., and W. Crawford (2000), Analysis of background free oscillations and how to improve resolution by subtracting the atmospheric pressure signal, *Phys. Earth Planet. Int.*, *121*, 325–338.

Row, R. V. (1966), Evidence of long-period acoustic-gravity waves launched into the *F* region by the Alaskan earthquake of March 28, 1964, *J. Geophys. Res.*, *71*, 343–345.

Row, R. V. (1967), Acoustic-gravity waves in the upper atmosphere due to a nuclear detonation and an earthquake, *J. Geophys. Res.*, *72*,1599–1610.

Saito, A., T. Tsugawa, Y. Otsuka, M. Nishioka, T. Iyemori, M. Matsumura, S. Saito, C. H. Chen, Y. Goi, and N. Choosakul (2011), Acoustic resonance and plasma depletion detected by GPS total electron content observation after the 2011 off the Pacific coast of Tohoku Earthquake, *Earth Planets Space*, *63*, 863867.

Smith, W., R. Scharroo, V. Titov, D. Arcas, and B. Arbic (2005), Satellite altimeters measure Tsunami, *Oceanography*, *18* (2), 102.

Song, Y. Tony, Chen Ji, L.-L. Fu, Victor Zlotnicki, C. K. Shum, Yuchan Yi, and Vala Hjorleifsdottir (2005), The 26 December 2004 tsunami source estimated from satellite radar altimetry and seismic waves, *Geophys. Res. Lett.*, *32*, L20601.

Suda, N., K. Nawa, and Y. Fukao (1998), Earth's background free oscillations, *Science*, *279*, 2085–2091.

Tanaka, T., T. Ichinose, T. Okuzawa, and T. Shibata (1984), HF-Doppler observations of acoustic waves excited by the Urakawa-Oki earthquake on 21 March 1982, *J. Atmospheric Terrest. Phys.*, *46*, 233–245.

Tanimoto, T., J. Um, K. Nishida, and N. Kobayashi (1998), Earth's continuous oscillations observed on seismically quiet days, *Geophys. Res. Lett.*, *25* (10), 1553–1556.

Tsai, H.F., J.-Y. Liu, C.-H. Lin, and C.-H. Chen (2011), Tracking the epicenter and the tsunami origin with GPS ionosphere observation, *Earth Planets Space*, *63*, 859–862.

Tsugawa, T., A. Saito, Y. Otsuka, M. Nishioka, T. Maruyama, H. Kato, T. Nagatsuma, and K. T. Murata (2011), Ionospheric disturbances detected by GPS total electron content observation after the 2011 off the Pacific coast of Tohoku Earthquake, *Earth Planets Space*, *63*, 875–879.

Vigny, C., W. J. F. Simons, S. Abu, R. Bamphenyu, C. Satirapod, N. Choosakul, C. Subarya, A. Socquet, K. Omar, H. Z. Abidin, and B. A. C. Ambrosius (2005), Insight into the 2004 Sumatra-Andaman earthquake from GPS measurement in southeast Asia, *Nature*, *436*, 201–206.

Watada, S. (1995), Part 1: Near-source acoustic coupling between the atmosphere and the solid Earth during volcanic eruptions, Ph. D. thesis, California Institute of Technology.

Watada, S. (2009), Radiation of acoustic and gravity waves and propagation of boundary waves in the stratified fluid from a time-varying bottom boundary, *J. Fluid Mech.*, *627*, 361–377.

Watada, S., and H. Kanamori (2010), Acoustic resonant oscillations between the atmosphere and the solid earth during the 1991 Mt. Pinatubo eruption, *J. Geophys. Res*., *115*, B12319, doi:10.1029/2010JB007747.

Webb, S. C. (2007), The Earth's "hum" is driven by ocean waves over the continental shelves, *Nature 445* (15 February), 754–756, doi:10.1038/nature05536.s.

Wei, S., R. Graves, D. Helmberger, J.-P. Avouac, and J. Jiang (2012), Sources of shaking and flooding during the Tohoku-Oki earthquake: A mixture of rupture styles, *Earth and Planetary Science Letters 333334* (2012) 91100.

Zurn, W., and R. Widmer, Worldwide observation of bichromatic long-period Rayleigh waves exited during the June 15, 1991, eruption of Mount Pinatubo, *Fire and Nud, eruption of Mount Pinatubo, Philippines*, 615–624. C. Newhall, R. Punongbayan J., Philippine Institute of Volcanology and Seismology, Quezo City and University of Washington Press.